Vanadium based XVO_3 (X = Na, K, Rb) as promising thermoelectric materials: First-principle DFT calculations

N A Noor[1,†], Nosheen Mushahid[1], Aslam Khan[2], Nessrin A. Kattan[3], Asif Mahmood[4,‡], and Shahid M. Ramay[5]

[1] *Department of Physics, University of Lahore, Lahore 54000, Pakistan*
[2] *Physics Department, KFUEIT, Rahim Yar Khan, Punjab, Pakistan*
[3] *Department of Physics, Faculty of Science, Taibah University, Medina, Saudi Arabia*
[4] *College of Engineering, Chemical Engineering Department, King Saud University Riyadh, Riyadh* 11451, *Saudi Arabia*
[5] *Department of Physics and Astronomy, College of Science, King Saud University Riyadh, Riyadh* 11451, *Saudi Arabia*

(Received 10 January 2020; revised manuscript received 27 May 2020; accepted manuscript online 5 June 2020)

We investigate structural, mechanical, thermodynamic, and thermoelectric properties of vanadium-based XVO_3 (X = Na, K, Rb) materials using density functional theory (DFT) based calculations. The structural and thermodynamic stabilities are probed by the tolerance factor (0.98, 1.01, and 1.02) with the negative value of enthalpy of formation. Mechanical properties are analyzed in the form of Born stability criteria, ductile/brittle nature (Poisson and Pugh's ratios) and anisotropy factor. To explore the electronic transport properties, we study the electrical conductivity, thermal conductivity, Seebeck coefficient and power factor in terms of chemical potential and temperature. High values of Seebeck coefficient at room temperature may find the potential of the studied perovskites in thermo-electrics devices.

Keywords: density functional theory, Born stability criteria, Seebeck coefficient, power factor

PACS: 71.15.–m, 72.20.Pa, 61.43.Bn, 31.15.A– **DOI:** 10.1088/1674-1056/ab99ad

1. Introduction

Perovskite materials have been recognized as possible low-cost materials owing to their tremendous applications in technologies and in industries. In the cubic unit cell of ABO_3 perovskites, A, B, and O have coordinates (0, 0, 0), (1/2, 1/2, 1/2) and (1/2, 1/2, 0), respectively.[1] In the family of perovskites, V-based compounds support an astounding variety of properties from metallic, insulating, and semiconducting behavior to ferroelectric, ferromagnetic, and potentially multiferroic phases.[2,3] Moreover, vanadium due to its variable oxidation states (3+, 4+, and 5+) along with its ability to make a strong bond with oxygen gives rise to particular physical properties and grow in a variety of crystalline structures.[4] The unique versatility of such an oxide perovskite crystal structure finds novel functionalities in material science and enormous potential for novel device applications.[5,6]

Shpanchenko *et al.*[7] and Belik *et al.*[8] reported that such materials undergo a unique transformation from metallic-like behavior to and insulator when they are exposed to high external pressure. Among transition metal oxides, AVO_3 ($3d^1$ electronic configuration) is a potential candidate for high-temperature solid oxide fuel cells, multiferroic devices and show novel applications in the field of high T_c superconductivity.[9] Regardless of their potential significance, appropriate investigations on the AVO_3 compounds are relativity rare. Thus, it is essential to investigate the numerous physical characteristics of AVO_3 (where A = alkali metal divalent cation) as well as their electronic structure. Sodium vanadate (NV) is an anti-ferroelectric material used in Na-ion batteries (NIBs) that have been considered best for energy storage systems due to the apparent advantages of indefinite Na resources and being inexpensive against the extensively used Li-ion batteries.[10,11]

Moreover, $NaVO_3$ has made a resurgence of research interest due to its considerable value of electric polarizations, the formation of short V–O bonds and significant off centering of the B-site sublattice.[12] We present some new insights into XVO_3 (X = Na, K, Rb) here as some new materials for energy-saving and light-emitting diodes.[13,14] Efficacious high-pressure development of AVO_3 (A = Na and Rb) with cubic structures was described earlier in the literature.[15,16] Our preeminent knowledge shows that no complete report is documented on cubic XVO_3 (X = Na, K, Rb) perovskites, which show influence of cationic distribution on the physical properties. This work analyze the mechanical, thermodynamic and thermoelectric properties of XVO_3, which are determined by using a density functional theory (DFT) that is eminent in finding the material properties of perovskites, best correlated with the experimental results.

†Corresponding author. E-mail: naveedcssp@gmail.com
‡Corresponding author. E-mail: ahayat@ksu.edu.sa

2. Method of calculations

The DFT calculations based on the Wien2k code[17] include all free and core electrons to execute electronic structures. This code is used to optimize and characterize the XVO_3-type perovskite oxides based on the full potential linearized augmented plane wave approach (FP-LAPW), in which the core region (muffin-tin) and interstitial region are treated under the influence of constant potential even though the solution to the Schrödinger wave equation is harmonic type in the core region and plane wave-like in the interstitial region. The studied oxides are optimized by Perdew–Burke–Ernzerhof (PBEsol-GGA)[18] for exact Hamiltonian calculation. Moreover, the energy is converged by most versatile Trans and Blaha modified Becke–Johnson potential (mBJ)[19,20] for exact band gap and electronic structures of studied oxides because the mBJ potential averages the deviations of LDA and GGA approximations.[21] The mBJ approach is used to investigate better and more reliable band structures in comparison to other approaches.[22–26]

For these calculations, we use R_{MT} (muffin-tin radius) and K_{Max} (wave vector in reciprocal lattice) as 8, while the Gaussian factor G_{max} and the angular momentum vector ℓ_{max} are taken as 16 units and 10 units, respectively. The most crucial factor is the selection of k-points/k-mesh for energy convergence. For optimization, we have made a k-mesh in different orders such as $10\times10\times10$, $12\times12\times12$, $15\times15\times15$, …, $30\times30\times30$. It is found that energy released during optimization increases up to the k-mesh in order of $30\times30\times30$ and then becomes constant. Therefore, we run all the calculations of optimization for ground state parameters and self-consistent field (SCF) for thermoelectric properties with $30\times30\times30$ k-point mesh. The size of the unit cell is in the order of $1\times1\times1$, and we take the energy released from the optimized system up to the accuracy of 4 digits (0.00001 Ryd/unit cell) during the iteration process. To find the thermoelectric response of the studied oxides, we use the BoltzTraP code[27] that is formulated according to classical Boltzmann transport theory. The parameters such as electrical conductivity σ, thermal conductivity κ, and Seebeck coefficient S obtained from BoltzTrap are scaled by the constant relaxation time of unity, their actual values should be estimated using an appropriate relaxation time, giving the temperature and carrier concentration. Furthermore, Chapin's method[28] for the solution to the tensor matrix of nonlinear first-order differential equations is used to calculate the elastic constant.

3. Results and discussion

The studied compounds are optimized to relax their cubic structures ($Pm\bar{3}m$, No. 221) and remove the strain forces involved in the structures. The optimized plots of these compounds are presented in Fig. 1(a) along with cubic structures in which alkali metals (Na, K and Rb)[29] are located at the edges of the cubic, the V atom is located at the central position of a tetrahedron of oxygen atoms (see Fig. 1(b)). It is clear from the optimized plots that lattice constant increases because of increasing the atomic radii of the alkali earth metals. The increasing lattice constant results in a decrease in bulk modulus. The calculated values of these parameters are listed in Table 1.

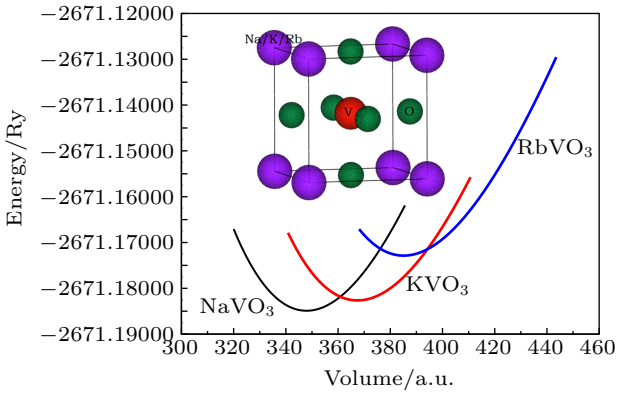

Fig. 1. Energy versus volume using PBEsol-GGA, and the optimized cubic structure (inset) using the Xcrysden software[29] for $NaVO_3$, KVO_3, and $RbVO_3$.

Table 1. The calculated lattice constant a_0 (Å), bulk modulus B_0 (GPa), tolerance factor t, enthalpy of formation ΔH (eV), elastic constant (C_{11} (GPa), C_{12} (GPa), C_{44} (GPa)), Shear modulus G (GPa), Young modulus Y (GPa), Pugh ratio B/G, and θ_D (K) of $NaVO_3$, KVO_3 and $RbVO_3$ in cubic phase by using the PBEsol-GGA approximation. TF(t_g): compatibility of an ion with perovskite crystal structure, with t_g being the Goldsmidth tolerance factor.

Parameters	$NaVO_3$	KVO_3	$RbVO_3$
a_0/Å	3.72	3.79	3.85
Other Calc.	3.68[a], 3.77[b]	3.75[a], 3.85[b]	3.91[b]
B_0/GPa	201	193	187
TF(t_g)	0.98	1.01	1.02
ΔH/eV	–2.32	–2.14	–2.08
C_{11}/GPa	304	311	279
C_{12}/GPa	130	123	126
C_{44}/GPa	99	124	136
B/GPa	188	186	177
G/GPa	94	112	112
Y/GPa	243	279	278
B/G	1.98	1.66	1.57
θ_D/K	747	765	658

[a]Ref. [47], [b]Ref. [48].

3.1. Structural and thermodynamic stability

The analyses of the XVO_3 (X = Na, K, Rb) perovskite oxides for device fabrication should concentrate on the structural and thermodynamic stability to improve its reliability. The

structural stability is ensured by the tolerance factor[30]

$$t_{\rm g} = 0.707 \frac{\langle r_X - r_{\rm O} \rangle}{\langle r_{\rm V} - r_{\rm O} \rangle}. \quad (1)$$

The X–O and V–O are the average bond lengths between atoms at the center of at octahedral and tetrahedral positions of oxygen. For cubic structures, the ideal range of tolerance factor is 0.94–1.02. Our calculated values of the tolerance factor lies in this range that ensures the studied oxides can be easily grown in the cubic phase (see Table 1). Moreover, the thermodynamic stability is also important for device reliability. Therefore, thermal stability is reported by the enthalpy of formation by[31]

$$\Delta H_{\rm f} = E_{\rm Total}\,(X_l {\rm V}_m {\rm O}_n) - lE_X - mE_{\rm V} - nE_{\rm O}, \quad (2)$$

where $E_{\rm Total}\,(X_l {\rm V}_m {\rm O}_n)$ is the total energy of the studied oxides while E_X, $E_{\rm V}$ and $E_{\rm O}$ are separated energies of X, V and O atoms, respectively. The negative formation energies of the perovskite oxides ensure that they are thermally stable in the existing cubic phase (see Table 1).

3.2. Mechanical and electronic properties

To know the mechanical behavior of the $X{\rm VO}_3$ (X = Na, K, Rb), the information of the elastic tensor matrix is necessary to generate three elastic constants C_{11}, C_{12}, and C_{44}, respectively. These three elastic constants explain complete mechanical behavior.[32] The mechanical stability of studied oxides is confirmed from the Born mechanical stability conditions on elastic constants ($C_{11} - C_{12} > 0, C_{44} > 0, C_{11} + 2C_{12} > 0$ and $C_{12} < B_0 < C_{11}$), and this approach has been used for numerous studies.[33–36] The elastic moduli (B, Y, and G) determine the tensile deformation, change in volume and shape of the studied oxides, when stress is applied on them. The values of B decreases while E and G increase, because of the increasing size of alkali metal ions (X). Furthermore, the bulk moduli obtained from elastic constants $B_0 = (C_{11} + 2C_{12})/3$ and optimization are equivalent, which shows that the DFT calculations are reliable. The ductile and brittle properties of the studied oxides are also important for device fabrication, analyzed from Poisson's ratio ν having critical limit $\nu = 0.26$ and the Pugh ratio B_0/G having critical limit $B_0/G = 1.75$.[37] Above these critical limits, the materials are ductile, and below them are brittle. Our reported values in Table 1 show that $NaVO_3$ is ductile, while $NaVO_3$ and $NaVO_3$ are brittle.

Furthermore, the specific heat capacity C_v, which measures how much heat a material can withstand without changing its phase, has been measured up to 900 K. The specific heat capacity also has electronic and lattice contribution like thermal conductivity, but we ignore the phonon contribution to make calculations simple and due to less contribution of phonons as compared to electrons. Figure 2(a) illustrates that with increasing temperature, the specific heat capacity increases. It is also noticed that the specific heat capacity of $RbVO_3$ is greater than the $NaVO_3$ and KVO_3. In high temperature region, C_v is well explained by the Einstein model, which could not meet the experimental function $C_v \propto T^3$, because of dominant behavior of acoustic phonons in the low-temperature range and out of phase vibrations.[38,39] Later on, the problem of low-temperature region has been solved by Debye considering the atomic vibrations are frequency dependent. These frequencies are joined to gather by the set of a large number of frequencies rather than a single frequency that meet exactly with experimental results.[40] The number electron density (see Fig. 2(b)) increases with increasing temperature that shows direct relation with specific heat capacity.

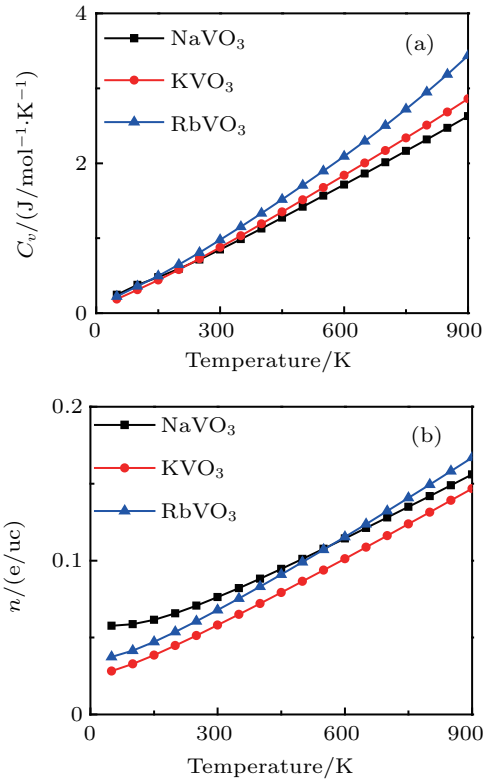

Fig. 2. (a) The calculated specific heat capacity and (b) the number electron density of $NaVO_3$, KVO_3, and $RbVO_3$ plotted against temperature.

The variation of lattice constant also affects the electronic structures and band gap of the studied compounds. The band gap decreases from $NaVO_3$ to $RbVO_3$ as shown in Fig. 3. The indirect nature of the band gap is due to the hybridization between electronic states of V in the conduction band and O in valence band along with the minor contribution of alkali metals (see Fig. 4). The indirect band gap involves the contribution of phonons that directly affect the thermoelectric properties, as discussed in the next part of this article.

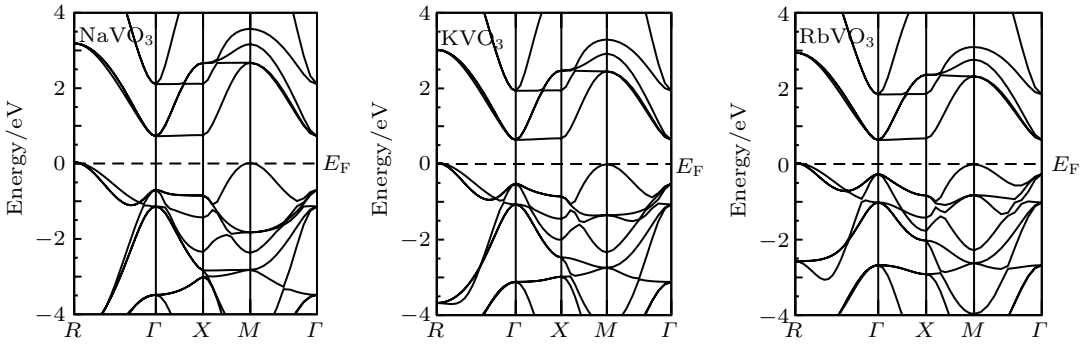

Fig. 3. Electronic band structures of $NaVO_3$, KVO_3, and $RbVO_3$ using mBJ.

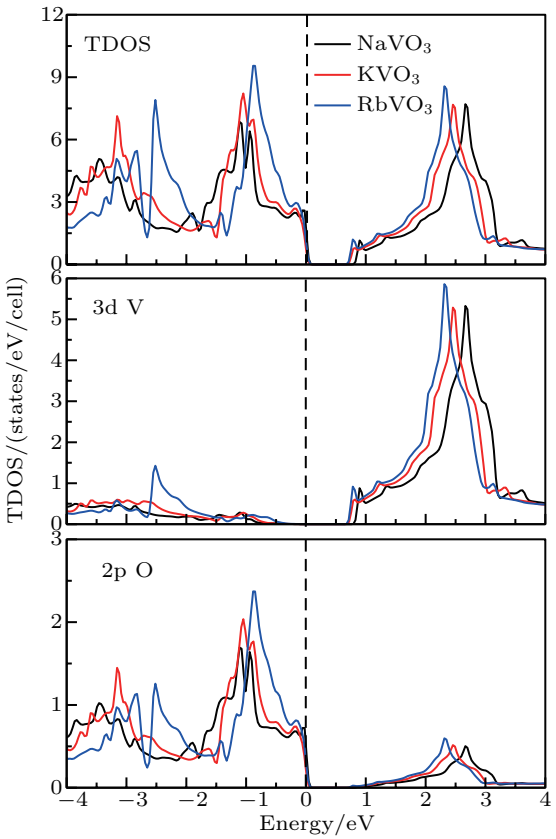

Fig. 4. The total density of states (TDOS) along with partial density of states (PDOS) calculated for $NaVO_3$, KVO_3 and $RbVO_3$ by using the mBJ potential.

3.3. Thermoelectric properties

The increase in energy consumption demands new sources of energy to fulfill the global shortage of energy. For this purpose, a variety of materials and methods are tested to dig out the cheap, economical and easy ways to produce the energy. The oxide-based compounds are useful in converting wasted heat into useful electrical energy due to high thermal stability and low lattice thermal conductivity.[41] Therefore, the thermoelectric behavior of the XVO_3 (where X = Na, K and Rb) has been analyzed with the electronic transport coefficients σ/τ, k_e/τ, and Seebeck coefficient S. The thermoelectric efficiency has been calculated from power factor $\sigma S^2/\tau$.[42–44] BoltzTraP simulations are trustworthy to predict electronic contributions to thermal transports under the umbrella of constant relaxation time approximation. One can use the deformation potential theory, whereas it always overestimates relaxation time because the theory accounts only the acoustical phonons in carrier scattering phenomena. Therefore, we have reported electronic coefficients with the influence of relaxation time (see Figs. 5 and 6) to help experimentalists to directly compare the reported values. Our calculated room-temperature values of σ/τ, k_e/τ, S, and $\sigma S^2/\tau$ are listed in Table 2.

Table 2. The calculated indirect bandgap E_g (eV) and room-temperature values of electrical conductivity σ, thermal conductivity κ and Seebeck coefficient S and power factor σS^2 of $NaVO_3$, KVO_3 and $RbVO_3$ perovskites.

Perovskites	E_g/eV	$(\sigma/\tau)/10^{18}$ $(\Omega\cdot m\cdot s)^{-1}$	$(k_e/\tau)/10^{14}$ W/m·K	$S/(\mu V/K)$	PF/10^{10} W/m·K^2·s
$NaVO_3$	0.7	20.0	2.27	145	41.8
KVO_3	0.6	13.8	1.87	169	39.1
$RbVO_3$	0.55	14.5	1.88	161	37.7

The calculated results against chemical potential and Kelvin temperature are presented in Figs. 5–7. The electrical conductivity depends upon the free carriers available for conduction, which discriminate them as n-type (electrons) and p-type (holes) semiconductors. The Fermi level lies the valence band edge, showing that the free holes for conduction are easily available than electrons. The electrical conductivity in the chemical potential ranges from −2 eV to 2 eV and temperature ranges in the range 0–900 K as shown in Figs. 5(a) and 5(b).

The chemical potential μ is the energy required to introduce or remove the electron by overcoming the Coulomb repulsive and attractive forces. The value of electrical conductivity increases up to −0.8 eV for all the studied oxides,

after it $NaVO_3$ reaches to the peak value 5.7×10^{20} $(\Omega{\cdot}m{\cdot}s)^{-1}$ at -1.3 eV. At the same time, for KVO_3 and $RbVO_3$, it decreases to 1.8×10^{20} $(\Omega{\cdot}m{\cdot}s)^{-1}$ and 1.5×10^{20} $(\Omega{\cdot}m{\cdot}s)^{-1}$ respectively, because of Coulomb repulsive and attractive forces provide different resistances to the movement of carriers (see Fig. 5(a)). For the positive value of chemical potential (n-type region), the carriers are electrons that increase the electrical conduction with increasing chemical potential linearly. Moreover, the temperature effect on electrical conduction shows the linearly increasing trend of electrical conductivity, because the electrons/holes at the higher temperature become more mobile for conduction. The slope of $NaVO_3$ has a greater value than KVO_3 and $RbVO_3$ because Na metal provides more electrons per unit cell.

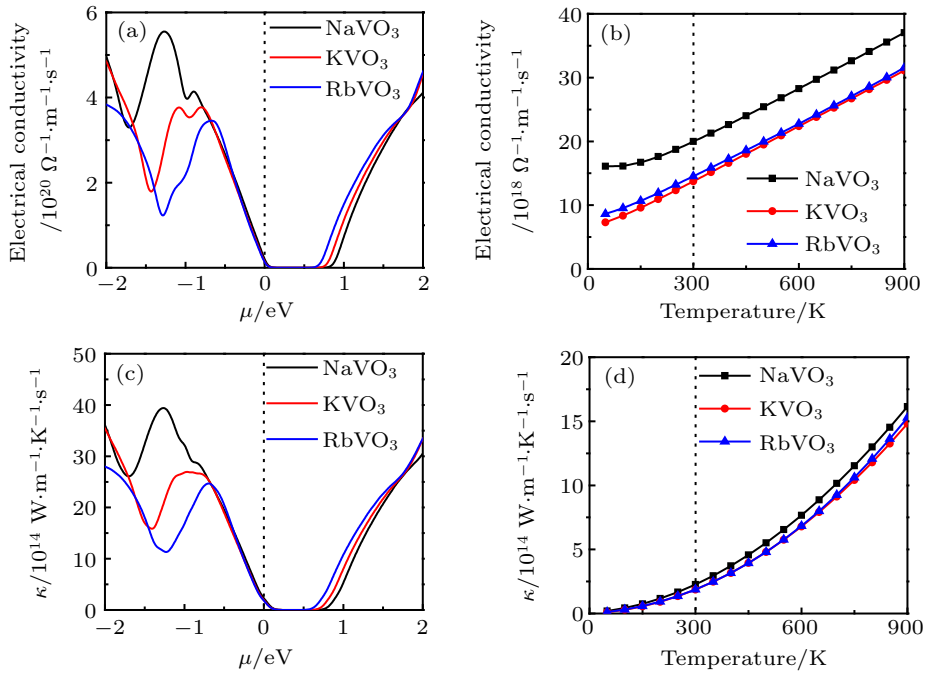

Fig. 5. The electrical and thermal conductivities of $NaVO_3$, KVO_3 and $RbVO_3$ against [(a), (c)] chemical potential and [(b), (d)] temperature, respectively.

The heat flow due to temperature change per unit length named as thermal conductivity and can be expressed by Fourier's law as $q = -k\nabla_x T$, where q, $\nabla_x T$ and k are heat efflux, temperature gradient and coefficient of thermal conductivity. Thermal conductivity has two parts: one is the electronic contribution k_e and the other is the lattice vibration k (phonons). In n-type or p-type semiconductors the carriers are available for conduction that depresses the lattice contribution. Therefore, we have elaborated the electronic part of thermal conductivity in the current report.

The calculated values of thermal conductivity versus chemical potential and temperature are presented in Figs. 5(c) and 5(d). The thermal conductivity follows the similar trend as electrical conductivity, but its value is small as compared to electrical conductivity to minimize the thermal-to-electrical conductivity as explained in the Wiedemann–Franz formula $LT = k/\sigma$, with the value in order of 10^{-6} that makes them applicable for thermoelectric applications.[45]

The temperature gradient of potential between different metallic contacts at $J = 0$ can be analyzed by the expression $J = -\sigma\nabla V - \sigma S\nabla T$, where J, ∇V and ∇T represent the current density, potential gradient and temperature gradient, respectively. For the equilibrium condition of zero current density, the Seebeck coefficient is derived as $\nabla V = -S\nabla T$, its value fluctuates from positive to negative in the n-type region and remain zero in the p-type region[46] because of mobile hole carriers for electrical conductivity as shown in Fig. 6(a). The Seebeck coefficient increases linearly with increase of temperature up to 300 K and then becomes almost constant with further increases of temperature up to 900 K. Moreover, the Seebeck coefficient is high for $RbVO_3$ than KVO_3 and $NaVO_3$ because of small electrical conductivity of $RbVO_3$ as shown in Fig. 6(b).

Thermoelectric efficiency can be measured by different scales like power factor σS^2, which gives the rough estimated value without including the thermal conductivity while the figure of merit measures the thermal efficiency by considering the thermal effect. Our calculated results are considered and approximated up to some extent because these do not include the phonon contribution. The reported power factor is reported in Fig. 7(c), which shows that it has maximum values in two regions: at zero chemical potential and at 1 eV because of the cooperative consequence of electrical conductivity and Seebeck coefficient. Furthermore, its value increases linearly with increasing temperature (see Fig. 7(a)).

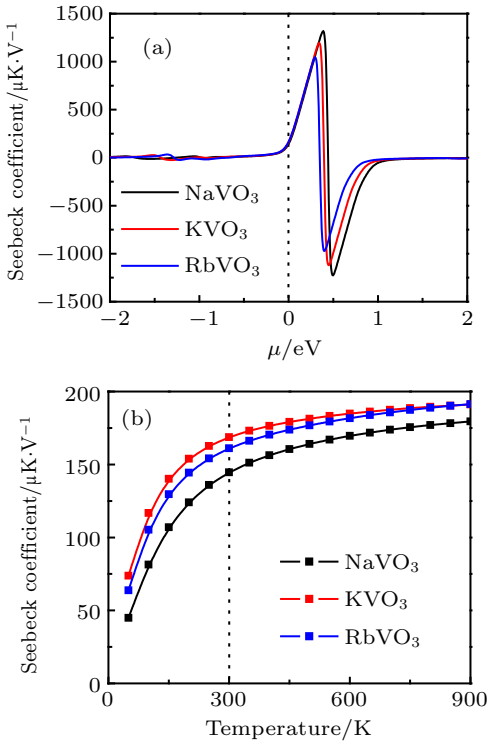

Fig. 6. The Seebeck coefficients S of $NaVO_3$, KVO_3, and $RbVO_3$ against (a) chemical potential and (b) temperature.

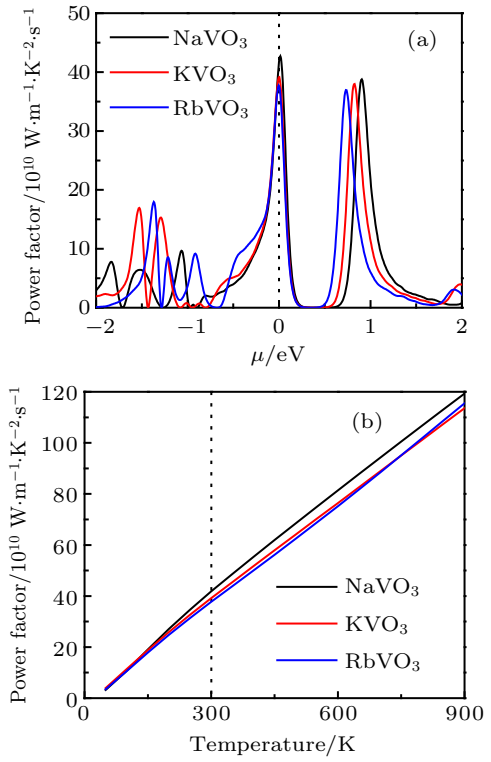

Fig. 7. The power factors $\sigma S^2/\tau$ of $NaVO_3$, KVO_3, and $RbVO_3$ against (a) chemical potential and (b) temperature.

The studied materials are low-cost oxides having high value of electrical conductivity due to the smaller band gaps. Therefore, they are suitable for thermoelectric applications. Moreover, they are mechanically stable and fulfill the essential condition of stability for the device applications.

4. Conclusions

In summary, we have investigated the structural, mechanical and thermoelectric properties of alkaline earth metal-based perovskites. The studied perovskites possess structural and thermodynamic stabilities as confirmed by a tolerance factor and enthalpy formation. Moreover, $NaVO_3$ is ductile while KVO_3 and $RbVO_3$ are brittle in nature. The room-temperature Seebeck coefficients of 145 μV/K, 169 μV/K, and 161 μV/K are obtained for $NaVO_3$, KVO_3, and $RbVO_3$, respectively. The $RbVO_3$ has a high value of thermal efficiency than $NaVO_3$ and KVO_3, because of its smaller band gap and high electrical conductivity.

Acknowledgment

The authors extend their appreciation to the Deanship of Scientific Research at King Saud University for funding the work through the research group project No. RGP-311.

References

[1] Lines M E and Glass A M 2001 *Principles and Applications of Ferroelectrics and Related Materials* (Oxford: Oxford University Press)
[2] Schindler M, Hawthorne F C and Baur W H 2000 *Chem. Mater.* **12** 1248
[3] Singh D J 2006 *Phys. Rev. B* **73** 094102
[4] Selbin J 1965 *Chem. Rev.* **65** 153
[5] Hawthorne F and Calvo C 1977 *J. Solid State Chem.* **22** 157
[6] Erum N and Iqbal M A 2017 *Chin. Phys. B* **26** 047102
[7] Shpanchenko R V, Chernaya V V, Tsirlin A A, Chizhov P S, Sklovsky D E, Antipov E V, Khlybov E P, Pomjakushin V, Balagurov A M, Medvedeva J E, Kaul E E and Geibel C 2004 *Chem. Mater.* **16** 3267
[8] Belik A A, Azuma M, Saito T, Shimakawa Y and Takano M 2005 *Chem. Mater.* **17** 269
[9] Hui S 2001 *Solid State Ionics* **143** 275
[10] Li Y, Lu Y, Zhao C, Hu Y S, Titirici M M, Li H, Huang X and Chen L 2017 *Energy Storage Mater.* **7** 130
[11] Larcher D and Tarascon J M 2015 *Nat. Chem.* **7** 19
[12] Ponomarev B K, Red'kin B S and Sinitsyn V V 2012 *Inorg. Mater.: Appl. Res.* **3** 338
[13] Nakajima T, Isobe M, Tsuchiya T, Ueda Y and Kumagai T 2008 *Nat. Mater.* **7** 735
[14] Nakajima T, Isobe M, Tsuchiya T, Ueda Y and Kumagai T 2009 *J. Lumin.* **129** 1598
[15] Belik A A and Takayama-Muromachi E 2006 *J. Solid State Chem.* **179** 1650
[16] Patwe S J and Rao U R K 1995 *J. Mater. Sci. Lett.* **14** 1702
[17] Blaha P, Schwarz K, Madsen G K H, Kvasnicka D and Luitz J 2001 *WIEN2K, An Augmented Plane Wave + local Orbitals Program for Calculating Crystal Properties* (Karlheinz Schwarz, Techn. Universiťat Wien Austria)
[18] Perdew J P, Ruzsinszky A, Csonka G I, Vydrov O A, Scuseria G E, Constantin L A, Zhou X and Burke K 2008 *Phys. Rev. Lett.* **100** 136406
[19] Tran F and Blaha P 2009 *Phys. Rev. Lett.* **102** 226401
[20] Koller D, Tran F and Blaha P 2011 *Phys. Rev. B* **83** 195134
[21] Perdew J P, Burke K and Ernzerhof M 1996 *Phys. Rev. Lett.* **77** 3865
[22] Saeed Y, Kachmar A and Carignano M A 2017 *J. Phys. Chem. C* **121** 1399
[23] Saeed Y, Singh N and Schwingenschlögl U 2012 *Adv. Functn. Mater.* **22** 2792
[24] Saeed Y, Singh N and Schwingenschlögl U 2014 *Appl. Phys. Lett.* **104** 033105
[25] Saeed Y, Singh N and Schwingenschlögl U 2014 *Appl. Phys Lett.* **105** 031915
[26] Singh N, Saeed Y and Schwingenschlögl U 2014 *Phys. Status Solidi RRL* **8** 849
[27] Madsen G K and Singh D J 2006 *Comput. Phys. Commun.* **175** 67

[28] Folland G B 1995 *Introduction to Partial Differential Equations* (Princeton: Princeton University Press)
[29] Kokalj A 1999 *J. Mol. Graph. Modell.* **17** 176
[30] Stoumpos C C, Cao D H, Clark D J *et al.* 2016 *Chem. Mater.* **28** 2852
[31] Topor L, Navrotsky A, Zhao Y and Weidner D J 1997 *J. Solid State Chem.* **132** 131
[32] Ji X, Yu Y, Ji J, Long J, Chen J and Liu D 2015 *J. Alloy Compd.* **623** 304
[33] Mahmood Q, Javed A, Murtaza G and Alay-E-Abbas S 2015 *Mater. Chem. Phys.* **162** 831
[34] Sajjad M, Alay-E-Abbas S, Zhang H, Noor N, Saeed Y, Shakir I and Shaukat A 2015 *J. Magn. Magn. Mater.* **390** 78
[35] Behram R B, Iqbal M, Alay-E-Abbas S, Sajjad M, Yaseen M, Arshad M I and Murtaza G 2016 *Mater. Sci. Semicond. Process.* **41** 297
[36] Nazir S, Mahmood I, Noor N, Laref A and Sajjad M 2019 *High Energy Density Phys.* **33** 100715
[37] Roknuzzaman M, Ostrikov K, Wang H, Du A and Tesfamichael T 2017 *Sci. Rep.* **7** 1
[38] Ciftci Y, Çolakoglu K, Deligoz E and Ozisik H 2008 *Mater. Chem. Phys.* **108** 120
[39] Hao Y J, Chen X R, Cui H L and Bai Y L 2006 *Physica B* **382** 118
[40] Noor N, Mahmood Q, Rashid M, Haq B U and Laref A 2018 *Ceram. Int.* **44** 13750
[41] Sajjad M, Singh N, Sattar S, Wolf S D and Schwingenschlögl U 2019 *ACS Appl. Energy Mater.* **2** 3004
[42] Hassan M, Shahid A and Mahmood Q 2018 *Solid State Commun.* **270** 92
[43] Sabir B, Murtaza G, Mahmood Q, Ahmad R and Bhamu K 2017 *Curr. Appl. Phys.* **17** 1539
[44] Majid F, Nasir M T, Algrafy E, Sajjad M, Noor N, Mahmood A and Ramay S M 2020 *J. Mater. Res. Techn.* **9** 6135
[45] Noor N A, Mahmood Q, Hassan M, Laref A, Rashid M 2018 *J. Mol. Graph. Modell.* **84** 152
[46] Yasukawa M, Ueda K, Fujitsu S and Hosono H 2017 *Ceram. Int.* **43** 9653
[47] Angsten T, Martin L W and Asta M 2018 *Chem. Mater.* **30** 587
[48] Saal J E, Kirklin S, Aykol M, Meredig B and Wolverton C 2013 *JOM* **65** 1501